

DOI: 10.1002/adma.200702353

Length Fractionation of Carbon Nanotubes Using Centrifugation**

By Jeffrey A. Fagan,* Matthew L. Becker, Jaehun Chun, and Erik K. Hobbie

Scalable manufacturing of single wall carbon nanotube (SWCNT) devices, sensors, and therapeutic agents will require precursors possessing well-defined length, chirality, and dispersion characteristics. However, existing synthetic and dispersion methods for SWCNTs produce heterogeneous mixtures of tube diameters, lengths and chiralities.^[1–8] As the unique optical, physical, thermal and electronic properties arise from the specific chiral wrapping vector of the graphene sheet,^[9] the necessity for separation of SWCNT materials by chirality is obvious. However, the strength and usability of these chirality specific properties also depends strongly on the length of the nanotube, and thus length fractionation is also desirable or required for many applications. The cost-effectiveness of performing both of these separations will determine the future utility of SWCNT based advanced technologies.

Recently, several methods have been described to enhance SWCNT population purity of individual SWCNT species. These include electrophoresis, dielectrophoresis, and ion exchange chromatography, which have all been demonstrated to separate tubes by diameter and electronic structure, although with limited throughput.^[10–14] Most recently, an article by Arnold et al.^[15] demonstrated the use of ultracentrifugation on single wall carbon nanotubes (SWCNTs) within a density gradient to produce a more facile and scalable, chirality separation. This significant advance works by driving the SWCNTs to their individual *equilibrium* locations within the density gradient.

Length separation has also been carried out using various chromatographic techniques, including gel electrophoresis and size exclusion chromatography (SEC), which yield populations possessing well-defined lengths and length distributions.^[16–20] While SEC methods are scalable in principle, lengths have

been limited in practice by the exclusion limit of the column stationary phase, which is generally less than 600 nm. In this contribution, we describe and demonstrate that ultracentrifugation can also be used to produce length fractionated SWCNTs in excess of 1 μm, using the same materials as Arnold et al., but by exploiting the *transient* motion of the SWCNTs in the dense liquid.

Since the development of the ultracentrifuge by Svedberg^[21,22] in the early 20th century, the separation of solutes with weak buoyancy differences has been feasible due to the enormous centripetal acceleration generated by such instruments. Arnold et al. recently exploited this to generate buoyancy driven chirality separations of surfactant covered single wall nanotubes by driving the SWCNTs to their equilibrium positions within a density gradient.^[15] However, the transient time period can also be exploited to yield separations. In the case of individually dispersed SWCNTs, differences in the scaling of the buoyancy and frictional forces allows for length separation of the nanotubes in this transient regime. Discounting convection of the fluid, a Nernst-Planck formulation can be used to model the flux, N_i , of each species i .

$$N_i = \frac{c_i F_{\text{buoyancy}}}{f_i} - D_i \nabla c_i \quad (1)$$

Here, c_i is the concentration, f_i is the friction factor and $D_i = k_B T / f_i$ the diffusion coefficient of species i ; k_B is Boltzmann's constant, T is the temperature, and $k_B T$ is the thermal energy of the solution. The buoyant force, F_{buoyancy} , is

$$F_{\text{buoyancy}} = \pi r^2 \ell * (\rho_s - \rho_{\text{SWCNT},i}) * G \quad (2)$$

in which r is the radius of the SWCNT *plus the surfactant shell*, ℓ is the tube length, ρ_s and $\rho_{\text{SWCNT},i}$ are the density of the solution and the SWCNT (plus its surfactant shell), respectively, and G is the centripetal acceleration. The length dependence of the friction factor suggests the possibility of length based separation. For a very long, thin rod the friction factor can be represented as^[23]

$$\begin{aligned} f_{\parallel} &\propto \frac{\pi \eta \ell}{\gamma} \left(\frac{1 + 0.307/\gamma}{1 - 0.5/\gamma} + 0.426/\gamma^2 \right), \\ f_{\perp} &\propto \frac{\pi \eta \ell}{\gamma} \left(\frac{1 + 0.307/\gamma}{1 + 0.5/\gamma} + 0.119/\gamma^2 \right) \end{aligned} \quad (3)$$

[*] Dr. J. A. Fagan, Dr. M. L. Becker, Dr. J. Chun, Dr. E. K. Hobbie
Polymers Division, National Institute of Standards and Technology
100 Bureau Drive, Gaithersburg, MD 20899 (USA)
E-mail: jeffrey.fagan@nist.gov

[**] The authors gratefully acknowledge the support of the National Institute of Standards and Technology, in funding this work through an Innovation in Measurement Science award. Support from a National Research Council – National Institute of Standards and Technology postdoctoral fellowship (J. A. F.) is gratefully acknowledged. This article, a contribution of the National Institute of Standards and Technology, is not subject to US copyright. Certain equipment and instruments or materials are identified in the paper to adequately specify the experimental details. Such identification does not imply recommendation by the National Institute of Standards and Technology, nor does it imply the materials are necessarily the best available for the purpose.

where η is the fluid viscosity and $\gamma = \ln(\ell/r)$. The constant of proportionality is 2 for motion parallel to the SWCNT axis and 4 for perpendicular motion. Given average parameters for ultracentrifugation

$$\left| c_i F_{\text{buoyancy}} / f_i \right| \gg |D_i \nabla c_i| \quad (4)$$

thus the diffusive component of the flux can be eliminated in combining Equations 1 to 3 to yield an equation for the flux of randomly oriented rods in which the nonlinear dependence on SWCNT length, approximately proportional to $\ln(\ell/r)$, is clearly apparent.

$$N_i(\ell) \approx c_i \frac{(\rho_s - \rho_{\text{SWCNT},i}) G r^2}{6\eta} \quad (5)$$

$$\frac{2\gamma^4 + 0.614\gamma^3 + 0.544\gamma^2 - 0.136\gamma}{\gamma^3 + 0.614\gamma^2 + 0.638\gamma - 0.135}$$

The consequence of Equation 5 is that longer SWCNTs travel with a greater velocity in opposition to the applied acceleration. Thus, the typical broad initial distribution can be separated by fractionating the liquid column after a set period of time determined by the length of material desired to be best resolved. The experimental procedure involves injection of the SWCNTs at an initial position, $z = 0$, into a fluid with a different density, and a centripetal acceleration equal to many times g (the acceleration due to gravity) is applied. Length separation, with minimal chirality differentiation, will occur in an experiment when $\Delta\rho = \rho_s - \langle \rho_{\text{SWCNT}} \rangle \gg \Delta\rho_{\text{SWCNT}} = \langle \rho_{\text{SWCNT}} \rangle - \rho_{\text{SWCNT},i}$ where $\rho_{\text{SWCNT},i}$ is the density of an individual SWCNT chirality, and $\langle \rho_{\text{SWCNT}} \rangle$ is the average density of all the SWCNT chiralities.

For the experiments, the density of the layers were chosen such that $\Delta\rho \gg \Delta\rho_{\text{SWCNT}}$ in the starting layer and for 5 cm above. Specifically, $\Delta\rho$ was $\approx 85 \text{ kg m}^{-3}$, while $\Delta\rho_{\text{SWCNT}}$ was $< 3 \text{ kg m}^{-3}$. The flux, N_i , of the individual nanotubes is therefore dominated by the length dependence of F_{buoyancy}/f_i .

Under the centrifugation conditions described in this work, nanotubes reached the top of the liquid column in less than 20 h, the time at which the solution volume was fractionated and the samples analyzed through ultraviolet-visible-near infrared spectroscopy (UV-Vis-NIR), dynamic light

scattering (DLS), and atomic force microscopy (AFM). As in Arnold et al.^[15], iodixanol (5,5'-[(2-hydroxy-1-3 propanediyl)-bis(acetylamino)] bis [N,N'-bis(2,3-dihydroxypropyl)-2,4,6-triiodo-1,3-benzenecarboxamide]), purchased as Opti-Prep, was used to generate the various density solutions. In the experiment described here, CoMoCat process SWCNTs were used, however the technique has been repeated with similar results using both laser and HiPco process SWCNTs.

A schematic of the experiment and spectra for several of the fractionated layers are shown in Figure 1. When run to optimize the transient motion of the SWCNTs, spectra showing well-defined SWCNT peak features with increasing peak to baseline ratios are measured above the injection layer. No significant presence of SWCNT bundles, as would be observed by a combination of peak broadening and decrease in peak absorption relative to the baseline, was observed for deoxycholate dispersed SWCNTs; a small amount of high density impurities is seen to fractionate through the dense underlayer to the bottom of the tube. In sodium cholate dispersions bundles are observed due to the significantly

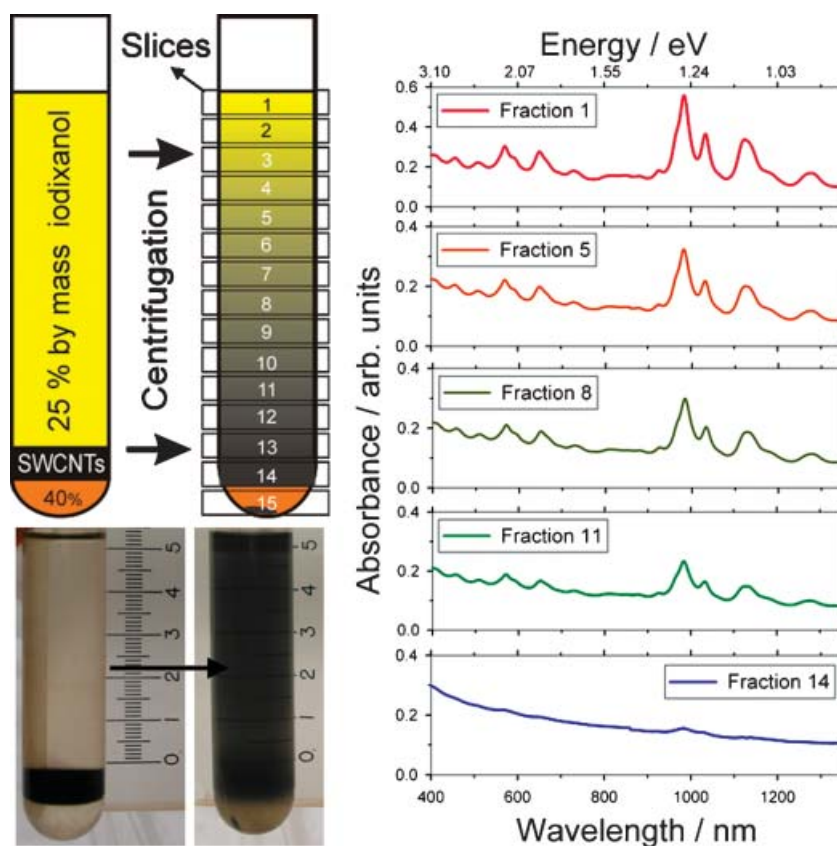


Figure 1. A diagram of the initial and final location of the CoMoCat SWCNTs, and UV-vis-NIR spectra for the indicated fractionation locations. The SWCNTs were injected in a 30% iodixanol mass fraction layer. The longer fractions display sharp SWCNT optical transitions with no evidence of significant chirality selection. Fractions at and below the injection layer have features that are smeared and red-shifted; this sort of absorption feature is indicative of bundling. The absorbance spectra below 375 nm and above 1300 nm contain contributions from the iodixanol that are difficult to subtract; these contributions negligibly affect the spectra in the (400 to 1300) nm range.

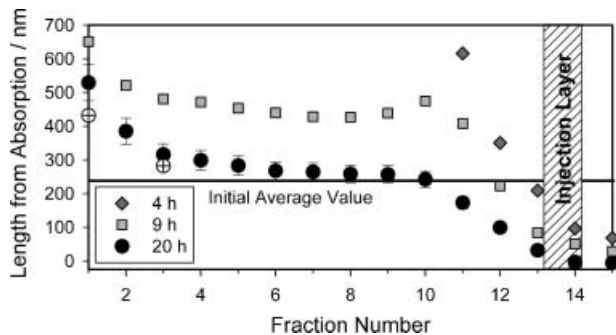


Figure 2. Apparent length versus fraction number at 4 h, 9 h, and 19 h of centrifugation. The peak height to baseline ratio for the same SWCNT material wrapped with DNA and length separated by size exclusion chromatography was also used to project the length of the nanotubes. Each fraction was 0.45 cm tall. Error bars represent 10% of the projected length value due to uncertainty in the slope of Equation 6. A change to this slope affects all projected values by a uniform multiplier. The crossed circles are AFM measured values for 20 h fractions; as overlapping tubes are not counted, AFM may underestimate the actual average length. Note that the concentration is not uniform across the fractions, and that the initial distribution of lengths is centered at ≈ 215 nm.

poorer stability of individual SWCNTs in sodium cholate solutions. In the deoxycholate results, no change in the chirality distribution with the length separation is measurable, as is evidenced by the constant relative sizes (to each other) of the chirality specific absorption features in Figure 1.

Lengths, shown in Figure 2, are projected from the measured absorption ratio of the 984 nm peak to an approximate baseline value measured at 775 nm. The length dependence based on this ratio was calculated from a linear fit to the same ratio versus length measured for DNA-dispersed CoMoCat SWCNTs length separated by size exclusion chromatography.^[18,24] An approximate relation for the length for this batch of CoMoCat SWCNTs is

$$\ell(\text{nm}) \approx \left(\frac{\text{Absorbance}(984 \text{ nm})}{\text{Absorbance}(775 \text{ nm})} - 0.842 \right) * 160.4 \text{ nm} \quad (6)$$

Values for the lengths measured using depolarized dynamic light scattering are in general agreement with the projected length values from the absorption. The large amount of iodixanol present in each fraction causes AFM measurement to be difficult. AFM measurements on the longest fraction isolated, and the corresponding absorption spectra (both shown in Fig. 3), yield lengths of (960 ± 35) nm based on 175 SWNTs and 1093 nm respectively, indicating that length extrapolation using the UV-Vis-NIR absorption is sufficiently accurate. Of note is that the peak to baseline ratio shown in Figure 3 is equivalent to the ratio calculable for the (6,5) purified samples shown in Arnold et al. Chirality purification of the sample shown in Figure 3 would thus yield spectra with substantially larger peak to baseline values than previously demonstrated in a bulk sample. Error bars for lengths

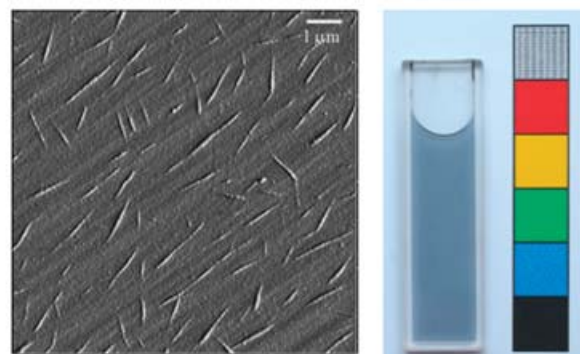
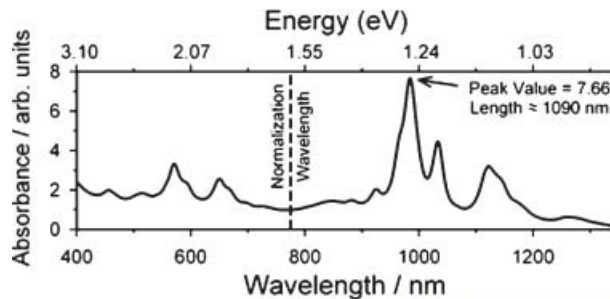


Figure 3. The spectra of the longest separated material has a peak height to baseline ratio ≈ 7.6 . This corresponds to a DNA-SWCNT calibrated length, via Equation 6, of 1090 nm. The average length measured via AFM (amplitude image shown) for this fraction is 960 nm with a standard deviation of the mean (SDOM) of 35 nm, indicating that length separation is both occurring, and that the lengths can be sufficiently be described by the DNA-SWCNT calibration. The small discrepancy in length for this specific fraction may be due to the small amount of chirality sorting apparent in the spectra, which would enhance the apparent optical length. The imaged fraction was collected from the top layer of the separation, this layer includes all lengths that have traveled that distance as the meniscus prevents the longest SWCNTs from traveling farther; this effect is the primary source of the polydispersity visible in the AFM. The photograph shows the color of the solution for the spectra shown.

calculated by Equation 6 are set to 10% of the average value, to project the estimated 10% uncertainty in the slope value.

Figure 4 shows the SWCNT length versus distance traveled for the experiment detailed in Figure 1. The lines are calculated length versus distance curves for the SWCNTs using Equation 4. The measured velocity indicates an effective diameter of $\approx (6$ to $13)$ nm for the SWCNT plus its surfactant shell, assuming that the effective buoyancy difference, $\Delta\rho$, is independent of the iodixanol concentration, and the equilibrium density value¹ of 1055 kg m^{-3} is used for $\langle\rho_{\text{SWCNT}}\rangle$. Such a value for the effective diameter could indicate that either the effective buoyancy of the SWCNTs varies with the iodixanol concentration, or that the presence of the iodixanol molecules increases the length scale of the surfactant structure around each SWCNT. A combination of the two effects is also a possibility. This finding may indicate that the iodixanol molecule is functional in producing the buoyant density shell around the nanotube. More research is required in this area. An interesting effect notable in Figure 4 is the sharp sigmoidal shape of the data. This effect is not noted for short time

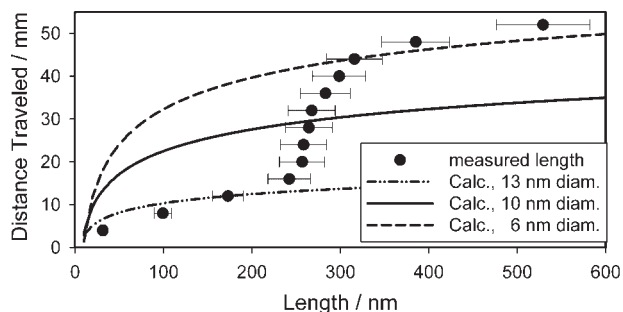


Figure 4. The theoretical SWCNT displacement calculated as a function of the nanotube length assuming a value of 3, 5, or 6.5 nm for the effective radius and the following parameters: $\Delta\rho = 83 \text{ kg/m}^3 \gg \Delta\rho_{\text{SWNT}}$, $\eta = 0.002 \text{ kg ms}^{-1}$, and $G = 40000 \text{ g}$. Translational diffusion can be shown to be unimportant for this calculation. Error bars in length represent 10% of the of the projected length value due to uncertainty in the slope of Equation 6, the uncertainty in the distance traveled is approximately equal to the point size. The curves likely do not overlap the data exactly due to unaccounted for phenomena, such as additional frictional drag from the sedimentation of the polymer, failure of the slender body approximation for shorter SWCNTs, possible relative alignment of longer SWCNTs due to motion or a sedimentation potential or surfactant driven effects (which could introduce a sigmoidal functionality to the theoretical curve), vibration driven mixing during the centrifugation, and the use of a non-optimal fixed angle rotor for the separation.

separations (as seen in Fig. 2), and is not captured by the first order theory given above. The physics causing this behavior are currently under investigation.

It is important to note that the length separation result presented here does not conflict with the results of Arnold et al.; given a proper density gradient above the injection layer the separation will run to the point at which the tube densities approach the local density within the gradient. In this situation $\Delta\rho_{\text{SWCNT}} = \langle\rho_{\text{SWCNT}}\rangle - \rho_{\text{SWCNT},i}$ becomes important and the SWCNTs fractionate by chirality. For length separation, the key is to exploit the transient motion regime, not the regime in which buoyancy equilibrium is approached.

In summary, ultracentrifugation can be used to separate single wall carbon nanotubes by length. In this experiment approximately 0.25 mg of dispersed CoMoCat SWCNTs were sorted by length in each of the identically prepared 15 mL centrifuge tubes, demonstrating that mg scale separation is easily obtainable. Future work will explore a switch to a swinging bucket rotor to provide a theoretically optimal geometry for the separation, as well as additional parameters of the separation. As noted by Arnold et al., commercial centrifuges are available that can handle 0.5 L or more, while generating $G > 150000 \text{ g}$, creating a strong potential for scale up.

Experimental

Materials: CoMoCat process SWCNTs were purchased from South-West Nanotechnologies (Norman, OK). Sodium deoxycholate and iodixanol were purchased from Fisher Scientific (Pittsburgh, PA) and Sigma-Aldrich (Milwaukee, WI) respectively and used as received.

Ultracentrifugation: Controlled length fractionation was achieved for HiPco, laser and CoMoCat process SWCNTs via ultracentrifugation; SWCNTs were dispersed with 2% by mass sodium deoxycholate surfactant. SWCNT prep consisted of sonication (tip sonicator, 0.32 cm, Thomas Scientific) of the SWCNT powder loaded at $(1.0 \pm 0.2) \text{ mg mL}^{-1}$ in the 2% surfactant solution in $\approx 8.5 \text{ mL}$ batches immersed in an ice water bath and tightly covered at 9 W of applied power for 2 h. Post-sonication, each suspension was centrifuged at 21000 g in 1.5 mL centrifuge tubes for 2 h and the supernatant removed; the resulting rich black liquid contains primarily individually dispersed SWCNTs. Density modified solutions were generated by mixing the appropriate surfactant or SWCNT solution with an iodixanol (OptiPrep, 60% mass by volume iodixanol) and 2% by mass sodium deoxycholate solution. Liquid layers were performed by careful layering in 15 mL polycarbonate centrifuge tubes. A Beckman-Coulter J2-21 centrifuge with a JA-20 rotor was used; suspensions were spun for 20 h at 20000 rpm, generating an average force of 32000 g with a maximum force of $\approx 45000 \text{ g}$. The individual fractions were collected by hand pipetting off each layer in 0.75 mL increments.

In determining the velocity of an individual SWNT, the velocity will be proportional to the difference in the specific density of each SWNT and the medium.

$$\Delta\rho_i = (\rho_s - \rho_{\text{SWCNT},i}) \quad (7)$$

From the point at which the nanotubes stop being buoyant (known from experiment to be $\approx 9\%$ to 10% iodixanol for deoxycholate dispersion), ρ_{SWCNT} values covering the entire diameter distribution of CoMoCats are ≈ 1053 to 1058 kg m^{-3} . This value range matches the stated isopycnic density of (6,5) SWNTs in Crochet et al. [25] and is consistent with the unstated ρ_{SWCNT} numbers of Arnold et al. [15]. In the reported experiments the density of the liquid, ρ_s , was set to $\approx 1137 \text{ kg m}^{-3}$. Thus across the entire diameter range of CoMoCats, the maximum difference in ρ_{SWCNT} was $\approx 5 \text{ kg m}^{-3}$, compared to a $\Delta\rho_i$ value of $\approx 85 \text{ kg m}^{-3}$. Thus any difference in velocity due to chirality effects was less than about 6%.

UV-Vis-NIR Spectrophotometry: UV-Vis-NIR was performed in transmission mode on a PerkinElmer Lambda 950 UV-Vis-NIR spectrophotometer over the range of (1350 to 350) nm. Measurements were typically performed on the extracted fractions in a 2 mm path length quartz cuvette. In all cases, the incident light was circularly polarized prior to the sample compartment, and the spectra corrected for both dark current and background. Data was recorded at 1 nm increments with an instrument integration time of at least 0.12 s per increment. The reference beam was left unobstructed, and the subtraction of the appropriate reference sample was performed during data reduction.

Atomic Force Microscopy: Tapping-mode atomic force microscopy (AFM) measurements were conducted in air using a Nanoscope IV system (Digital Instruments) operated under ambient conditions with 1–10 $\Omega \text{ cm}$, phosphorous (*n*) doped silicon tips (Veeco; RTESP5, 125 μm length; 30 μm width, normal spring constant, 40 N m^{-1} ; resonance frequency, 240 kHz to 300 kHz). Length separated surfactant-coated tubes were diluted 100 \times in water ($18 \text{ M}\Omega \text{ cm}^{-1}$) prior to being deposited (2 μL) onto plasma cleansed Si [1,1,1] wafers. After being allowed to dry, the entire sample was exposed to high intensity UV light for 2 h followed by 1 isopropanol and 3 water wash cycles using a solution deposition/wicking procedure to afford clear imaging conditions.

Received: September 17, 2007

Revised: November 16, 2007

Published online: April 15, 2008

-
- [1] B. Kitiyanan, W. E. Alvarez, J. H. Harwell, D. E. Resasco, *Chem. Phys. Lett.* **2000**, *317*, 497.
- [2] M. J. Bronikowski, P. A. Willis, D. T. Colbert, K. A. Smith, R. E. Smalley, *J. Vac. Sci. Technol. A* **2001**, *19*, 1800.
- [3] R. C. Haddon, J. Sippel, A. G. Rinzler, F. Papadimitrakopoulos, *MRS Bull.* **2004**, *29*, 252.
- [4] J. A. Fagan, B. J. Landi, I. Mandelbaum, J. R. Simpson, V. Bajpai, B. J. Bauer, K. Migler, A. R. H. Walker, R. Raffaele, E. K. Hobbie, *J. Phys. Chem. B* **2006**, *110*, 23801.
- [5] B. J. Bauer, E. K. Hobbie, M. L. Becker, *Macromolecules* **2006**, *39*, 2637.
- [6] H. Wang, W. Zhou, D. L. Ho, K. I. Winey, J. E. Fischer, C. J. Glinka, E. K. Hobbie, *Nano Lett.* **2004**, *4*, 1789.
- [7] D. Wang, L. Chen, *Nano Lett.* **2007**, *7*(6), 1480.
- [8] W. Wenseleers, I. I. Vlasov, E. Goovaerts, E. D. Obraztsova, A. S. Lobach, A. Bouwen, *Adv. Funct. Mater.* **2004**, *14*, 1105.
- [9] J. W. G. Wildoer, L. C. Venema, A. G. Rinzler, R. E. Smalley, C. Dekker, *Nature* **1998**, *391*, 59.
- [10] M. Zheng, E. D. Semke, *J. Am. Chem. Soc.* **2007**, *129*, 6084.
- [11] M. Zheng, A. Jagota, E. D. Semke, B. A. Diner, R. S. McLean, S. R. Lustig, R. E. Richardson, N. G. Tassi, *Nat. Mater.* **2003**, *2*, 338.
- [12] S. K. Doorn, M. S. Strano, M. J. O'Connell, E. H. Haroz, K. L. Rialon, R. H. Hauge, R. E. Smalley, *J. Phys. Chem. B* **2003**, *107*, 6063.
- [13] R. Krupke, F. Hennrich, H. von Lohneysen, M. M. Kappes, *Science* **2003**, *301*, 344.
- [14] S. R. Lustig, A. Jagota, C. Khripin, M. Zheng, *J. Phys. Chem. B* **2005**, *109*, 2559.
- [15] M. S. Arnold, A. A. Green, J. F. Hulvat, S. I. Stupp, M. C. Hersam, *Nat. Nanotechnol.* **2006**, *1*, 60.
- [16] D. A. Heller, R. M. Mayrhofer, S. Baik, Y. V. Grinkova, M. L. Usrey, M. S. Strano, *J. Am. Chem. Soc.* **2006**, *126*, 14567.
- [17] C. A. Dyke, M. P. Stewart, J. M. Tour, *J. Am. Chem. Soc.* **2005**, *127*, 4497.
- [18] X. Y. Huang, R. S. McLean, M. Zheng, *Anal. Chem.* **2005**, *77*, 6225.
- [19] D. Chattopadhyay, S. Lastella, S. Kim, F. Papadimitrakopoulos, *J. Am. Chem. Soc.* **2002**, *124*, 728.
- [20] B. J. Bauer, M. L. Becker, V. Bajpai, J. A. Fagan, E. K. Hobbie, K. Migler, C. M. Guttman, W. R. Blair, *J. Phys. Chem. C* **2007**, *111*, 17914.
- [21] T. Svedberg, H. Rinde, *J. Am. Chem. Soc.* **1924**, *46*, 2677.
- [22] T. Svedberg, K. O. Pedersen, *The Ultracentrifuge*, Oxford University Press, London **1940**.
- [23] G. K. Batchelor, *J. Fluid Mech.* **1970**, *44*, 419.
- [24] J. A. Fagan, J. R. Simpson, B. J. Bauer, S. Lacerda, M. L. Becker, J. Chun, K. B. Migler, A. R. Hight Walker, E. K. Hobbie, *J. Am. Chem. Soc.* **2007**, *129*(34), 10607.
- [25] J. Crochet, M. Clemens, T. Hertel, *J. Am. Chem. Soc.* **2007**, *129*(26), 8058.
-